Double porous poly (-caprolactone)/chitosan membrane scaffolds as niches for human mesenchymal stem cells

Pritam Das, Simona Salerno, Jean-Christophe Remigy, Jean-Francois Lahitte, Patrice Bacchin, Loredana de Bartolo

Double porous poly (Ɛ-caprolactone)/chitosan membrane scaffolds as niches for human mesenchymal stem cells

Pritam Das[a,b], Simona Salerno[b], Jean-Christophe Remigy[a], Jean-François Lahitte[a], Patrice Bacchin[a,*], Loredana De Bartolo[b,*]

[a] Laboratoire de Génie Chimique, Université de Toulouse, CNRS UMR 5503, INPT, UPS, Toulouse, France
[b] Institute on Membrane Technology, National Research Council of Italy, ITM-CNR, c/o University of Calabria, via P. Bucci, cubo 17/C, I-87036, Rende (CS), Italy

ARTICLE INFO

Keywords:
Double porous membrane scaffold
Polycaprolactone-chitosan
Mesenchymal stem cells
Proliferation
Invasion
Oxygen consumption

ABSTRACT

In this paper, we developed membrane scaffolds to mimic the biochemical and biophysical properties of human mesenchymal stem cell (hMSC) niches to help direct self-renewal and proliferation providing to cells all necessary chemical, mechanical and topographical cues. The strategy was to create three-dimensional membrane scaffolds with double porosity, able to promote the mass transfer of nutrients and to entrap cells. We developed poly (Ɛ-caprolactone) (PCL)/chitosan (CHT) blend membranes consisting of double porous morphology: (i) surface macrovoids (big pores) which could be easily accessible for hMSCs invasion and proliferation; (ii) interconnected microporous network to transfer essential nutrients, oxygen, growth factors between the macrovoids and throughout the scaffolds. We varied the mean macrovoid size, effective surface area and surface morphology by varying the PCL/CHT blend composition (100/0, 90/10, 80/20, 70/30). Membranes exhibited macrovoids connected with each other through a microporous network; macrovoids size increased by increasing the CHT wt%. Cells adhered on the surfaces of PCL/CHT 100/0 and PCL/CHT 90/10 membranes, that are characterized by a high effective surface area and small macrovoids while PCL/CHT 80/20 and PCL/CHT 70/30 membranes with large macrovoids and low effective surface area entrapped cells inside macrovoids.

The scaffolds were able to create a permissive environment for hMSC adhesion and invasion promoting viability and metabolism, which are important for the maintenance of cell integrity. We found a relationship between hMSCs proliferation and oxygen uptake rate with surface mean macrovoid size and effective surface area. The macrovoids enabled the cell invasion into the membrane and the microporosity ensured an adequate diffusive mass transfer of nutrients and metabolites, which are essential for the long-term maintenance of cell viability and functions.

1. Introduction

An important challenge in tissue engineering and regenerative medicine is the design of a biomaterial able to provide all necessary physical, chemical and mechanical cues that promote cell colonization and tissue regeneration. Design approach for biomaterials are driven to the interest to reproduce the natural niche of cells that implies cell-cell and cell-extracellular matrix (ECM) contacts in a 3-D environment which ensure both the maintenance of cell polarity and cell-cell biochemical communication. In this context, a great interest is focused on the development of materials able to boost the proliferation and maintenance of mesenchymal stem cells (MSCs) secreting a broad spectrum of macromolecules [1,2] which represent a promising source for cell therapy and regenerative medicine. It has been reported that the hMSCs viability and functions highly depend on environmental cues such as oxygen and nutrient availability, pore size, scaffold mechanical property, surface morphology and more notably the administration of soluble factors [3,4]. Moreover, the hMSCs incorporation in a three-dimensional bulk environment, that ensure the mass transfer of nutrients and growth factors to and from the entrapped cells, represents a further challenging strategy in next advanced co-culture systems with other target cells. Microporous membranes with suitable topographical, mechanical, physico-chemical and permeability properties can act as an artificial stem cell niche providing a bio-instructive extracellular environment characterized by micro- and nano-architecture [5,6]. Membranes enable to provide an adequate structure in terms of porosity and interconnected pores, which is important for the selective mass transfer of nutrients and metabolites, and on the other hand favour cell

* Corresponding author.
E-mail addresses: bacchin@chimie.ups-tlse.fr (P. Bacchin), l.debartolo@itm.cnr.it, loredana.debartolo@cnr.it (L. De Bartolo).

https://doi.org/10.1016/j.colsurfb.2019.110493

attachment on the surface and invasion inside the bulk, increasing the effective area for cell accommodation [7,8]. However, this balance between the optimal pore size and effective cell adhesion area is often compromised in the case of small pores suitable for the transfer of nutrients, growth factors and waste products that limit the cell proliferation to the surface. Conversely, in the case of big pores, it implies an increase of area for cell invasion and migration within the bulk limiting the selective transport of molecules and the initial interaction with the surface, which is crucial to mediate all subsequent events such as proliferation and differentiation [9,10]. Big pores are also responsible to reduce the mechanical strength and can drive a faster degradation in vivo before finishing the tissue construct. To overcome these drawbacks, membranes with double porosity can be a further step forward where the macrovoids (big pores) are responsible for the invasion and proliferation of the cells, and the transport of nutrients and growth factors can be accomplished by interconnected micropores, resulting a higher effective surface area than a single big porous surface. Previously, we developed a polysulfone (PSU) membrane with double porosity level for cell culture that supported only partially the cell adhesion and migration owing to the hydrophobic and non-degradable character of the PSU [11]. Based on this previous concept here we developed more biocompatible and biodegradable membranes with double porosity through the modified liquid induced phase inversion process, by applying commercial track-etched membrane. The idea was to create new blended double porous membranes that can combine the features of chitosan (CHT) (e.g., bioactive functionality, hydrophilicity, degradation rate, chemical structure resemblance of the native tissue ECM) and polycaprolactone (PCL) (e.g., good mechanical properties, easy processing ability) [12–14], reducing the limitations of a single component and providing a greater level of control over the overall material properties for cell guidance and biocompatibility [15,16]. Interestingly, the bioactive functionality, biocompatibility, degradation and mechanical properties of the polymeric PCL-CHT blends have disclosed promising results in comparison to that on the separate culturing substratum [12–14]. Membranes must have an appropriate architecture to host cells at high density and to ensure an adequate transport of nutrients and metabolites [17,18]. To achieve this goal, membranes should have macrovoids to accommodate cells, and a microporosity for diffusion of nutrients. These requirements are essential for cell nutrition, proliferation and invasion inside the bulk for vascularization and formation of new tissues. For the first time we report here the design and application of a 3D double porous membrane scaffold of PCL-CHT prepared by modified liquid induced phase inversion technique for the culture of hMSCs. The scaffolds consist of macrovoids (22–46 μm) which are open towards the surface for cell proliferation and invasion, and interconnected micropores to transfer essential nutrients, growth factors and cell catabolites. Membranes were characterised in order to evaluate the structural, mechanical and physico-chemical properties before their use in contact with cells. In particular, we explored the capability of the double porous membranes to create a physical and chemical niche for hMSCs through investigation of cell adhesion, proliferation and invasion as well as the metabolic oxygen requirements.

2. Materials and methods

2.1. Membrane fabrication with 3D double porosity

The membranes were prepared using a liquid induced modified phase inversion technique by diffusion between solvent as formic acid (FA)/acetic acid (AA) mixture and non-solvent NaOH solution. In particular, poly (Ɛ-caprolactone) (MW 80 KDa, CAPA™ 6800, Perstorp Holding AB, Sweden) and CHT (MW 190–310 KDa, 75–85 % degree of de-acetylation, Sigma-Aldrich), with ratio 100/0 (15 wt%), 90/10 (14 wt%), 80/20 (14 wt%) and 70/30 (10 wt%) (w/w %) were dissolved in FA/AA (w/w %) mixture until complete dissolution. The polymer solutions were individually cast on a glass plate by a handle-casting knife in order to achieve a thickness of 250 μm, at room temperature. Then the track-etched membrane, a polyethylene terephthalate (PET) isoporous membrane (Sterlitech, USA) with pore diameter 10 μm, was rinsed by the solvent, slowly wiped to remove excess solvent, and gently applied on the casted polymer solution (Fig. S1).

The glass plate was then slowly immersed inside the non-solvent bath containing NaOH aqueous solution at room temperature. Just after immersion, solvent exchange started by forming a flat sheet membrane due to de-mixing of the polymer solution. A homogeneous solvent-exchange, on the casted solution not covered by the track-etched membrane, led to a single and closed porous structure. On the other hand, two different solvent-exchange rates took place in polymer solution covered by the track-etched membrane, which led to the double porous morphology. The macrovoids were formed where the non-solvent could manage a direct access inside the casted solution through the pores of the track-etched membrane and an interconnected microporous network was formed where the non-solvent was not able to make a direct entry.

CHT was dissolved in the solvent at 55 °C for 12 h. PCL was successively added when the temperature was below 35 °C. Within 2 h a clear, viscous and a faint yellow solution was obtained. After mixing, the polymeric solutions were kept in stand for 10–20 min and then cast. Due to high viscosity of CHT in the solvent, it was quite difficult to make a homogeneous solution by mechanical stirrer condition with PCL/CHT ratio beyond 70/30, which could cause phase segregation between the two polymers. Double porous membrane formation with pure CHT was also not possible as dissolving CHT more than 4 wt% was difficult by mechanical stirring condition and that wt % is not enough to make a practically workable membrane due to lack of good entanglement between the polymer chain.

After formation of the membrane the track-etched membrane was removed gently and the newly formed membrane was washed several times in pure water. Then, the membranes were stored in ultrapure water at 4 °C temperature. The surface where the macrovoids were open towards the non-solvent are denoted as top surface and the other surface, which was facing the glass plate, denoted as the bottom surface.

2.2. Membrane characterization

After the preparation, membranes were characterised in order to determine their morphological, physico-chemical, permeability and mechanical property.

The surface morphology and cross section were analysed by scanning electron microscopy (SEM, Quanta 200F, FEI, USA). Diameter of the macrovoids and micropore size distribution were evaluated by ImageJ software on the SEM images by considering at least 10 micrographs of each membrane with minimum average area 10^4 μm^2. The mean diameter of the passing pores was determined by Capillary Flow Porometer (CFP 1500 AEXL, Porous Materials Inc., PMI, Ithaca, New York, USA).

The membrane permeability was evaluated in an Amicon cell by pure water flux ($J_{solvent}$) measurements in the absence of solutes and at transmembrane pressures (ΔP^{TM}) ranging from 20 to 60 kPa. The hydraulic permeance Lp was measured assuming a linear correlation between the water flux ($J_{solvent}$) and the convective driving force, according the equation:

$$Lp = (J_{solvent}/\Delta P^{TM})_{\Delta c = 0}. \quad (1)$$

The mechanical properties were determined by Zwich/Roell Z2.5 tensile testing machine (Germany), by applying a pre-load of 0.05 MPa at constant 4 mm/min elongation rate [13]. Tensile strength (N/mm^2), Young's modulus E (N/mm^2) and elongation at break ε (%) were determined at room temperature on ten different samples (1 × 5 cm) from each batch, considering the different cross-section thickness, in dry and

wet conditions. Wet samples were analysed after an incubation of 6 h in PBS buffer. Real-time longitudinal deformation measurements were obtained and analysed by testXpert® testing software.

The membrane biodegradation was evaluated by enzymatic incubation in two different solutions of Lipase from *Aspergillus oryzae* (0.12 U/ml) and human Lysozyme (1300 U/ml), respectively, in PBS buffer and 0.5 mg/ml NaN_3, to emulate the enzymatic activities of human serum [19]. Before the incubation, three different samples (2 × 1.5 cm) from each batch were dried in vacuum oven at 37 °C for 72 h and then their initial weight (W_i) precisely measured. Then the samples were immersed in 1 ml of enzymatic solutions that were freshly changed every seven days. At predetermined time intervals, the samples were washed with copious distilled water, dried in vacuum oven at 37 °C for 72 h, and their final weight (W_f) precisely measured. The weight loss index (W_{loss} %) was determined by the following equation:

$$W_{loss} = \frac{W_i - W_f}{W_i} \times 100 \quad (2)$$

2.3. Cell culture

Human bone marrow mesenchymal stem cells (hMSCs) StemPro™ BM (Thermo Fisher Scientific) were cultured on sterilised double porous membranes with culture medium constituted by MesenPRO RS™ (Thermo Fisher Scientific) supplemented with 2 mM glutamine, 1% gentamycin sulphate/amphotericin-B, and 2% serum. hMSCs were seeded on the membrane scaffolds at $3.5*10^3$ cell/cm^2 density, and incubated at 37 °C in a 5% CO_2/20% O_2 atmosphere (v/v) with 95% relative humidity. Culture medium was changed every 48 h, and cells maintained up to 21 days.

2.3.1. Effective surface area (ESA%) for cell viability

We determined the effective surface area (ESA%) on the SEM images of the scaffolds by imageJ analysis. We calculated the total area of the macrovoids on a unit surface and subtract it from the total unit surface area as follows:

$$\begin{aligned} &Effective\ \ surface\ \ area\ \ (ESA\,\%) \\ &= \left(\frac{\begin{array}{l} Total\ \ unit\ \ surface\ \ area \\ -\ Total\ \ area\ \ of\ the\ \ macrovoids\ \ on\ \ that\ surface \end{array}}{Total\ unit\ \ surface\ \ area} \right) \times 100 \end{aligned} \quad (3)$$

2.3.2. Cell morphology

Cell morphology was investigated after 7 and 21 days of culture on double porous membrane scaffolds by Scanning Electron Microscopy and Confocal Laser Scanning Microscopy.

hMSCs were examined by SEM (SEM, Quanta 200F, FEI, USA) after proper fixation and dehydration, as previously described [1]. Samples were gently washed with PBS buffer, and then incubated for 30 min in 3% glutaraldehyde and 1% formaldehyde mixture. Successively, they were fixed for 30 min in 1% OsO_4, and progressively dehydrated in ethanol solutions.

For Confocal Laser Scanning Microscopy (CLSM, Fluoview FV300, Olympus Italia) analysis hMSCs were immunostained for specific markers [12]. In order to visualize the cell distribution on the membranes, the cytoskeleton protein vimentin and cell surface antigen CD90 were stained. Vimentin was stained by using a rabbit polyclonal anti-human vimentin (Santa Cruz Biotechnology, Santa Cruz, CA), and a Cy™2-conjugated AffiniPure donkey anti-rabbit IgG (Jackson ImmunoResearch Europe Ltd., Cambridge, UK); CD90 was marked by using a mouse monoclonal anti-human CD90 (eBioscience, San Diego, CA), and a Cy™3-conjugated AffiniPure donkey anti-mouse IgG (Jackson ImmunoResearch Europe Ltd., Cambridge, UK). Primary antibodies were incubated overnight at 4 °C, the secondary ones for 2 h at room temperature. Counterstaining of nuclei was performed with 0.2 μg/ml of 4′,6-diamidin-2 phenyl indole (DAPI) (Molecular Probes Inc., Eugene, OR) for 30 min.

The presence of hMSCs inside the macrovoids of the double porous membranes and the change of cell morphology from the surface towards the bulk of the membrane scaffolds were monitored with scan depth determination by CLSM in the z-scan mode (step size: 0.5 μm) (Fluoview 5.0 software, Olympus Corporation). Quantitative measurements of cell invasion and cell morphology along the z-axis were calculated by image analysis of CLSM micrographs (Fluoview 5.0 software, Olympus Corporation). Cell invasion was reported in terms of percentage of cell distribution on the top surface and in the bulk, at a distance of 15 μm. The change in cell morphology was measured and reported as frequency of cell surface area, by analysing overlapped CLSM images from all the double porous membrane scaffolds.

2.3.3. Cell proliferation

Cell viability and proliferation was assessed by the 3-(4,5-dimethylthiazol-2-yl)-2,5 diphenyl tetrazolium bromide (MTT) assay. After 7, 14 and 21 days of culture on the different double porous membranes, hMSCs were incubated in 5 mg/ml of MTT solution for 4 h at 37 °C. The yellow tetrazolium MTT salt was reduced by the mitochondrial dehydrogenase in living cells to purple formazan crystals. This precipitate was extracted by using 1 ml per sample of a lysis solution constituted of 10% sodium dodecyl sulphate, 0.6% acetic acid in DMSO, in mild stirring for 30 min at 37 °C. Then formazan product was quantified by spectrophotometry at 570 nm wavelength.

2.3.4. Oxygen uptake rate (OUR) measurements

The Oxygen uptake rate (OUR) of hMSCs cultured on the different double porous membrane scaffolds was continuously monitored up to 21 days by the pre-calibrated sensor dish reader (SDR; OxoDish®-DW, PreSens Precision Sensing GmbH), a high-throughput, 24-channel reader for non-invasive detection of O_2 in special multi-dishes. O_2 detecting sensors, placed at the bottom of each well, and containing a luminescent dye, were excited every 5 min by the SDR placed below the multi-dish. The luminescence lifetime was read out noninvasively through the transparent bottom, and the dissolved oxygen detected with a resolution of ± 0.4% O_2 at 20.9% O_2, and a response time < 30 s. Tests were done in the 24 well special multi-dishes in which samples with cells and samples without cells (as controls) were placed.

2.4. Statistical analysis

All tests were performed in triplicate and repeated three times. Data are reported as mean ± standard deviation. Statistical significance of collected data was determined according to ANOVA followed by Bonferroni *t*-test ($p < 0.05$).

3. Results

3.1. Membrane properties

The developed membrane scaffolds displayed different morphological, physico-chemical, mechanical, permeability and biodegradation properties (Table 1). SEM images revealed on the top surface macrovoids that are interconnected with a highly microporous spongy network (Fig. 1). Macrovoids with mean size of 13 ± 4 μm were found on PCL double porous membrane. The increase of CHT concentration in the polymeric blend increased gradually the mean diameter of macrovoids at the active surface to values of 15 ± 5 μm, 21 ± 11 μm and 35 ± 25 μm for PCL/CHT 90/10, PCL/CHT 80/20 and PCL/CHT 70/30, respectively (Table 1). The cross section of the membranes revealed inside the bulk macrovoids with bigger volume and mean diameters of

Table 1
Morphological, physico-chemical and mechanical properties of the PCL/CHT double porous membranes. Data statistically significant according to ANOVA followed by Bonferroni t'test ($p < 0.05$): (*) vs PCL/CHT 80/20 and 70/30; (θ) vs PCL/CHT 70/30; (§) vs all; (◊) vs PCL/CHT 100/0 and 90/10; (‡) vs PCL/CHT 100/0; (†) vs PCL/CHT 80/20.

PCL/CHT ratio	100/0	90/10	80/20	70/30
Polymer wt (%)	15	14	14	10
Macrovoids Diameter (μm)	13 ± 4 (surface)	15 ± 5 (surface)	21 ± 11 (surface)	35 ± 25$^{◊}$ (surface)
	22 ± 3 (bulk)	34 ± 10‡ (bulk)	27 ± 13 (bulk)	46 ± 4§ (bulk)
Mean Flow Pore Diameter (μm)	0.02	0.07	0.05	1.55
Effective Surface Area (%)	88 ± 1.0*	84 ± 1.0*	74 ± 2.0^{θ}	69 ± 2.0
Porosity (%)	40 ± 1.3	45 ± 1.2	48 ± 1.9‡	56 ± 5.0§
Thickness (μm)	45 ± 0.9	50 ± 1.0‡	60 ± 0.4§	55 ± 0.6$^{◊}$
Tensile Modulus E (N/mm^2)	143.6 ± 14.1§ (dry)	128.2 ± 4.8† (dry)	125.3 ± 11.8 (dry)	111.9 ± 4.6† (dry)
	131.6 ± 2.2§ (wet)	58.5 ± 4.1* (wet)	29.5 ± 0.8^{θ} (wet)	10.1 ± 2.7 (wet)
Ultimate Tensile Strenght Rm (N/mm^2)	8.3 ± 0.7§ (dry)	3.7 ± 0.4* (dry)	2.4 ± 0.2^{θ} (dry)	2.1 ± 0.2 (dry)
	8.1 ± 0.2§ (wet)	2.5 ± 0.3* (wet)	1.3 ± 0.1^{θ} (wet)	0.5 ± 0.2 (wet)
Elongation at break ε (%)	127.6 ± 50§ (dry)	13.1 ± 2.2 (dry)	6.9 ± 0.8 (dry)	2.1 ± 0.4 (dry)
	146.9 ± 68.4§ (wet)	17.6 ± 8.8 (wet)	15.8 ± 5.1 (wet)	9.1 ± 1.2 (wet)
Hydraulic Permeance (m/Pa s 10^{-5})	0.1 ± 0.001	0.11 ± 0.002	0.14 ± 0.003	0.19 ± 0.004

22 ± 3 μm, 34 ± 10 μm, 27 ± 13 μm and 46 ± 4 μm for PCL/CHT 100/0, PCL/CHT 90/10, PCL/CHT 80/20 and PCL/CHT 70/30, respectively. Interconnected micropores in the range of 1–5 μm were visible for all membranes and size distribution become wider with the increase of CHT concentration in the blended membranes (Fig. S2). Mean passing pore diameters of 0.02 μm, 0.07 μm, 0.05 μm and 1.55 μm were measured by capillary flow porometer for PCL/CHT 100/0, PCL/CHT 90/10, PCL/CHT 80/20 and PCL/CHT 70/30 membranes, respectively. Consistently the surface porosity was also depending on the ratio of CHT reaching values of 56% for PCL/CHT 70/30 membranes. The observed steady-state hydraulic permeance of the membranes calculated as slope of the pure water flux measurements versus transmembrane pressure (ΔP™) straightline follows the same trends of pore size and porosity: membrane permeability increased with increasing pore size and porosity, as expected.

Depending upon the mean macrovoids size and their density on the surface area, we calculated the effective surface area (ESA%) to relate to the cell adhesion and proliferation. We found a decrease of ESA with increasing the percentage of CHT reaching values ranging from 88 ± 1% for PCL/CHT 100/0 to 69 ± 2% for PCL/CHT 70/30 membranes.

The mechanical properties of the membranes evaluated in dry and in wet conditions are reported in Table 1. PCL/CHT 100/0 membranes displayed stable elastic properties in both dry and wet conditions, as evidenced by the moderate tensile modulus E (143.6 ± 14.1 and 131.6 ± 2.2 N/mm^2 in dry and wet conditions, respectively) in combination with elongation at break higher than 100%. The increase of CHT wt% in the blended membranes caused a gradual decrease of all the mechanical properties, including the tensile modulus, with respect to the pure PCL ones, reaching low values on the membrane of PCL/CHT 70/30, as a result of the gain of more fragile properties. Passing from the dry to the wet conditions, the tensile modulus and the ultimate tensile strength decreased, and the elongation at break increased (Table 1).

The biodegradable properties of the membranes were investigated by using separately lipase and lysozyme solutions at concentrations similar to human serum. The weight loss of all membranes increased with time as shown in Fig. 2. As expected, the degradation of membranes augmented with the decrease of PCL concentration giving rise the highest percentage of weight loss with the PCL/CHT 70/30 membranes. The membrane weight loss in lipase solution was quite fast and higher than that in lysozyme solution. After 17 days of incubation in lipase the blended PCL/CHT membranes were completely degraded. On the contrary, low percentage of weight loss was measured in lysozyme solution.

3.2. Adhesion and invasion of hMSCs in the double porous membranes

The capability of the developed membranes to promote the adhesion, invasion and proliferation of mesenchymal stem cells was evaluated in the culture time. Cells adhered over the membrane surfaces and appeared flattened with elongated filopodia as highlighted by SEM's images (Fig. 3). During the culture time they proliferated covering the membrane surfaces as shown in Fig. 3. In the case of PCL/CHT 100/0 and PCL/CHT 90/10 the hMSCs adhered on the surface and exhibited a spindle-like morphology. On the other two membranes (PCL/CHT 80/20 and PCL/CHT 70/30), which are characterised by large macrovoids at the surface (21 and 35 μm, respectively) and smaller effective surface area, cells beside adhere to the surface they were entrapped into the macrovoids and displayed a more spherical shape.

We investigated the expression of CD90 and vimentin as specific markers of undifferentiated status and proliferation/migration capability of MSCs, respectively. Cells on all investigated membranes were positive for the cytoskeleton protein vimentin (in green) and cell surface protein CD90 (in red) (Fig. 4). In agreements with the SEM observations, here we also found that cells attached to PCL/CHT 100/0 and PCL/CHT 90/10 surfaces exhibited a high degree of spreading. It is interesting to note that in the case of PCL/CHT 80/20 and PCL/CHT 70/30 membranes the most of cells were entrapped inside the macrovoids and acquired a globular morphology due to the limited area available for cell adhesion and organization. Since the spreading is characterized by a substantial flattening of the cells and an increase in overall surface area we evaluated the distribution of the cell surface area on the different membranes (Fig. 5). The frequency distribution of the cell surface area confirmed that on PCL/CHT 100/0 and 90/10 the most of cells achieved a very widely surface area (between 2400 and 5000 μm^2) on the contrary on PCL/CHT 80/20 and 70/30 a peak of surface area is around 60–100 μm^2 as an indication of unspread cells entrapped inside the macrovoids.

For a deeper understanding of the cell invasion phenomenon inside the scaffolds, we accrued the CLSM images in z-scanning mode from surface towards the bulk (Fig. 6). Quantitative image analysis established that 95 ± 1.8% and 97 ± 2.2% of cells adhered on the surface of PCL/CHT 100/0 and PCL/CHT 90/10 membranes, respectively, and few cells invaded the bulk. On the other hand, on PCL/CHT 80/20 and PCL/CHT 70/30 cells were distributed on both surface and bulk, acquiring spread and globular morphology, respectively. We calculated 16 ± 0.4% and 15 ± 3.1% of cells on PCL/CHT 80/20 and PCL/CHT 70/30 surfaces, respectively. For both membrane scaffolds 84 ± 0.4% and 85 ± 3.1% of cells were inside the bulk, at a distance of 15 μm from the top surface of PCL/CHT 80/20 and PCL/CHT 70/30 membranes. Moreover, the cell invasion in the latter two scaffolds increased

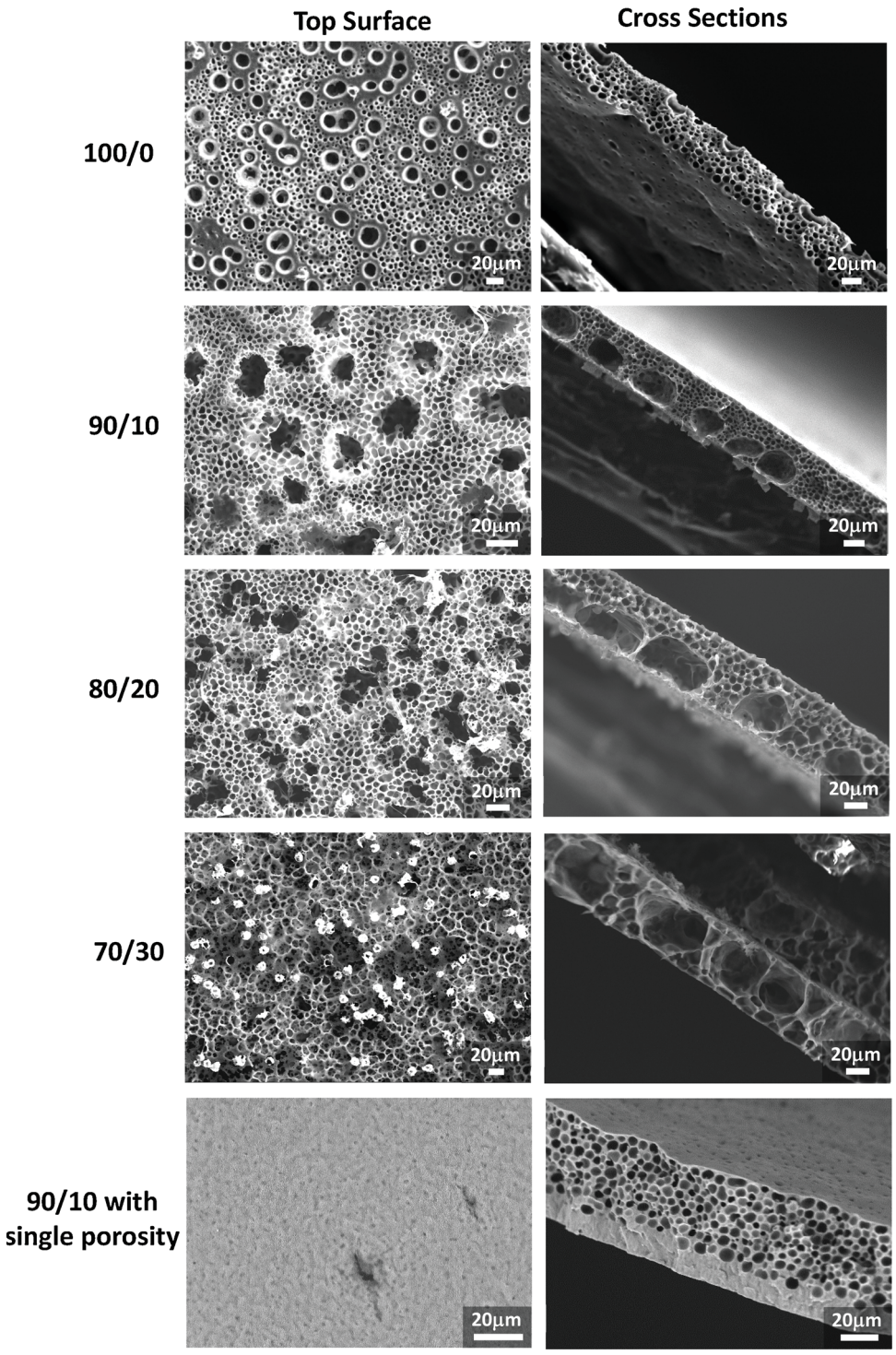

Fig. 1. SEM images: top surface and cross sections of PCL/CHT double porous membranes made by using the track-etched membrane, and with single porosity made without the track-etched membrane.

from 7 days to 21 days.

3.3. Cell proliferation and oxygen uptake rate of hMSCs in the double porous membranes

The cell experiment results demonstrated a remarkable effect of macrovoids size and surface morphology on cell proliferation and behaviour. Fig. 7a reports the quantitative cell viability by MTT assay after 7, 14 and 21 days. Here we found that cells grew on all membranes, especially on PCL/CHT 100/0 that showed the highest rate of cell viability after 14 days. The cell growth was slower on membranes with high CHT wt% that are characterised by greater mean macrovoid size and surface porosity. However, after 21 days all the membranes (except PCL/CHT 70/30) displayed almost similar cell viability. This result suggests that the scaffolds created a permissive microenvironment for hMSCs and after 21 days they reached confluence on the surface, even if differences in cell proliferation rates were observed as a function of macrovoids size and surface porosity.

Considering that oxygen deficiency is a serious problem for the cells and inadequate oxygenation induces a decrease of cell metabolism, we

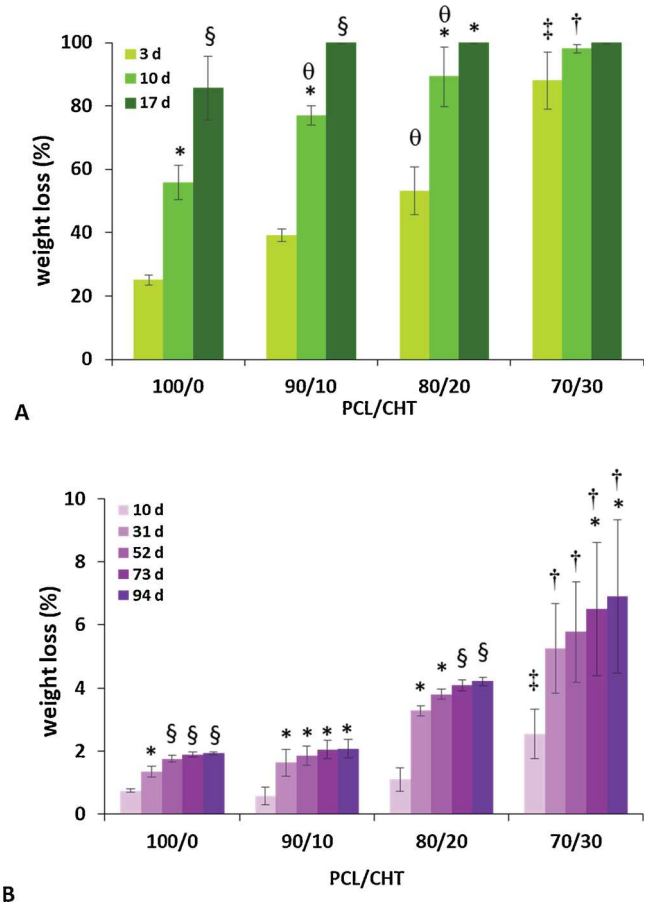

Fig. 2. Weight loss (%) of PCL/CHT double porous membranes with different time interval (days) by enzymatic degradation in presence of Lipase (*Aspergillus oryzae*with 0.112 U/ml) (A) and Lysozyme (0.013 mg/ml) (B). Data statistically significant according to ANOVA followed by Bonferroni t'test ($p < 0.05$): A) (*) vs 7 days, (§) vs 7 and 14 days, on the same substrate; (θ) vs PCL/CHT 100/0, (†) vs PCL/CHT 100/0 and 90/10, (‡) vs all, at the same day of culture. B) (*) vs 10 days, (§) vs 10 and 31 days, on the same substrate; (†) vs PCL/CHT 100/0 and 90/10, (‡) vs all, at the same day of culture.

evaluated the cellular oxygen uptake rate (OUR) with time until 21 days in Fig. 7b. Cells on PCL/CHT 100/0 displayed the highest OUR rate followed by PCL/CHT 90/10, which was also increased with time compared to the other two blended membranes. For PCL/CHT 80/20 and PCL/CHT 70/30 the oxygen consumption remained significantly high throughout experiment. The OUR values of the different blends after 20 days reached values of 38 ± 7 µmol/L min, 33 ± 2 µmol/L min, 15 ± 3 µmol/L min and 10 ± 2 µmol/L min for PCL/CHT 100/0, PCL/CHT 90/10, PCL/CHT 80/20 and PCL/CHT 70/30 membranes, respectively.

These results are in agreement with the proliferation data and SEM images that clearly indicate a very high density of the hMSCs on the surface of PCL/CHT 100/0 followed by PCL/CHT 90/10, without significant dead cell fragments.

4. Discussion

The design of bioactive membrane scaffolds mimicking the physiologic environment during tissue formation is an important challenge in biomaterials and tissue engineering research. Herein, we developed double porous polymeric membrane scaffolds that recapitulate the 3D microenvironment, able to ensure the long-term stem cell viability and metabolism. A distinguishing feature of the scaffolds is the combination of macrovoids that allow the cell entrapment with a small interconnected microporous network that ensures the selective transfer of oxygen and nutrients and the removal of cell catabolites and products. By changing the CHT wt%, not only the chemical properties of the scaffolds were varied, but also their permeability and structural properties like macrovoid size, effective surface area, surface porosity and surface regularity was also modified. Finally, all these properties had a direct and strong influence on the morpho-functional behaviour of hMSCs. The formation of the unique double porous morphology by modified non-solvent induced phase inversion is due to the track-etched membrane placement on the casted solution that produced two different solvent-exchange rates. The pores of the track-etched membrane restricted the non-solvent entry inside the casted polymer, leading to the formation of macrovoids [11]. The addition and increase of CHT wt % enhanced the viscosity of the casted solution inducing consequently an increase of the macrovoids size in the bulk with respect to the opening ones on the surface. On the contrary, without the use of the commercial track-etched membrane, the phase inversion was quite homogeneous leading to a single porous morphology without macrovoids, followed by dense skin formation [11,20].

The polymer composition influenced mechanical, physico-chemical and degradation properties as well as the surface morphology and macrovoid size of the developed membrane scaffolds. The mechanical behaviour of PCL was modified by introducing and increasing CHT wt %, that leads to an increase of the macrovoids size and the porosity, and consequently to a decrease of the polymers bulk density in unit volume. From these data an intrinsic correlation between hydraulic performance and structural properties of the membranes emerge. The larger mean pore size and porosity of the 70/30 PCL/CHT membrane is responsible for a hydraulic permeance almost 2 times higher than that measured for the 100/0 one.

The double porosity affected the tensile strength of all membranes [21], and was responsible of the decrease of the E modulus even in the blended membrane scaffolds, despite the introduction of the stiffer polymer chitosan. Moreover, the decrease of the tensile strength and Young's modulus could be due to the thermodynamic miscibility of the two polymers that affects their interfacial adhesion in contact surface and the yield strength of the matrix [22]. Additionally, in wet condition the mechanical properties dramatically change for double porous blended membranes owing to an incorporation of water molecules inside the bulk, through the macrovoids and among the polymeric chains. Water incorporation re-established new hydrogen bonds with the CHT polar functional groups, by disabling the previous polymer-polymer interaction to some extent and leading polymers to slide over another under stress. This phenomenon was previously observed also in CHT and PCL/CHT nanoporous membranes, and is responsible for reduced tensile strength and Young's modulus, and for increased elongation at break, in wet condition and increasing CHT wt% [12,13].

The enzymatic degradation is a very important physiological phenomenon which ensures enhanced cell-cell connection followed by tissue formation with time inside a 3D biodegradable scaffold. Particularly, lipase and lysozyme with human serum concentration simulated the physiological conditions that would be responsible for enzymatic dissolution of the different double porous membrane scaffolds in vivo as artificial patch [23]. Lipase mainly degrades PCL and polymeric chains that consists of lipid or ester-like chemical structure; lysozyme mainly degrades CHT consisting of *N*-acetyl/deacetyl glucosamine linkages via oxidative-reductive chain scission, with a degradation kinetic that is inversely related to the deacetylation degree of CHT [24]. The slower degradation rate in lysozyme is mainly due to the different degradation mechanism and the lower CHT wt% in all blends [25]. Nevertheless, the overall enzymatic degradation phenomenon was further governed by the easy accessibility of the enzymatic solution throughout the bulk, which could be beneficial for a scaffold with fast cell growth, needing the scaffold to degrade faster while being replaced by cell-secreted ECM [26]. In particular, the lower lipase degradation of PCL/CHT 100/0 could be due to a higher difficulty of water-soluble

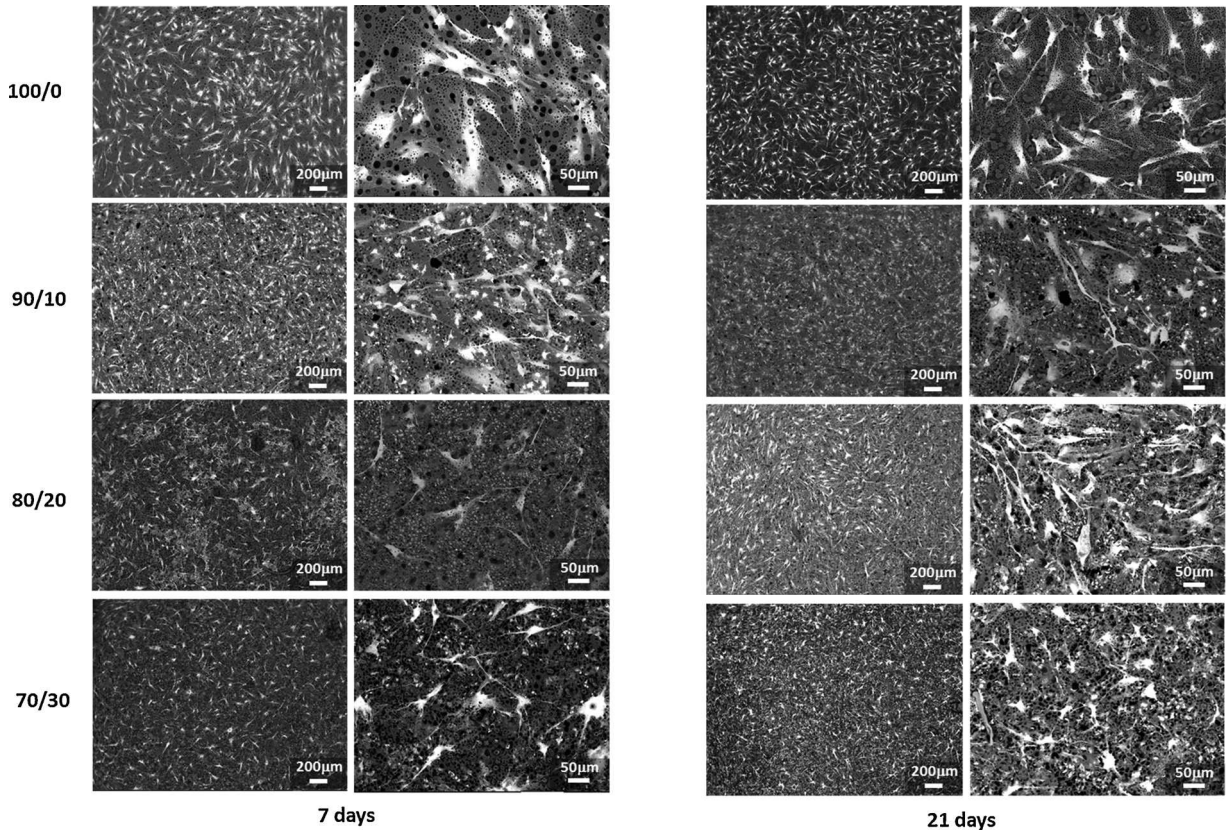

Fig. 3. SEM micrographs of hMSCs after 7 and 21 days of culture on PCL/CHT double porous membranes at different magnification.

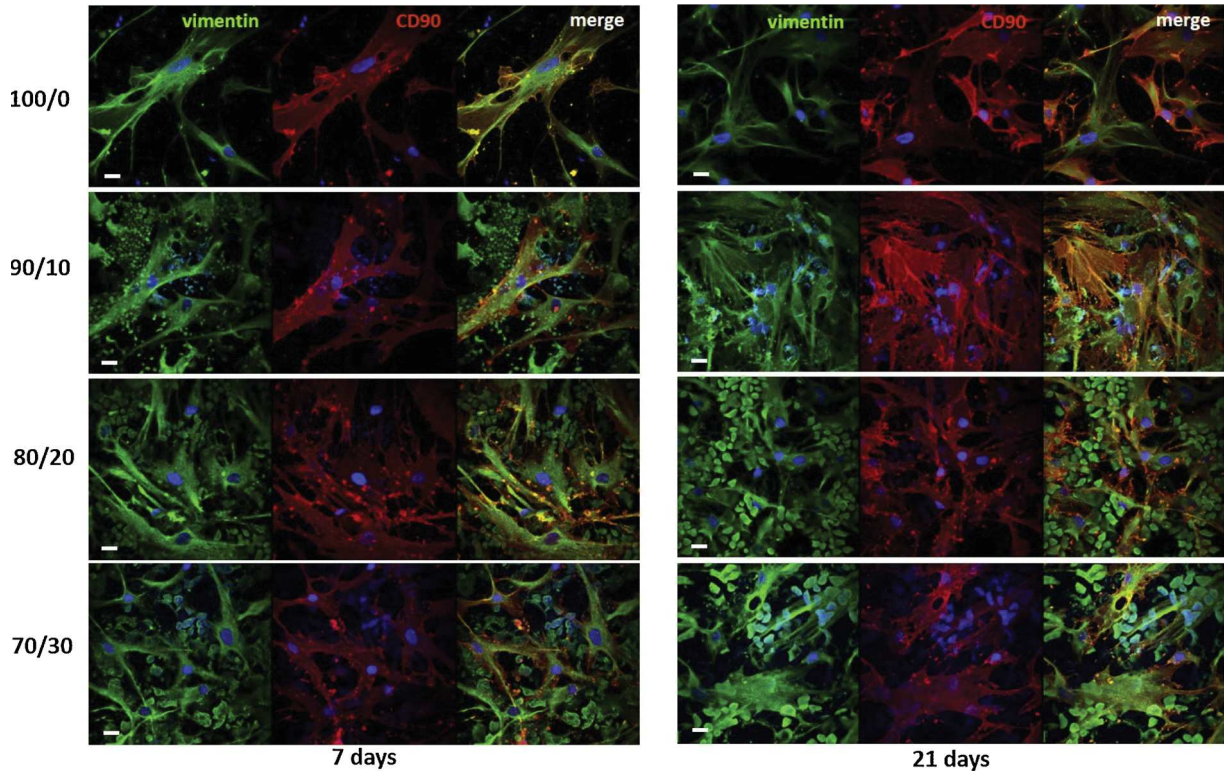

Fig. 4. CLSM images of hMSCs after 7 and 21 days of culture on PCL/CHT double porous membranes. Cells were stained for vimentin (green), CD90 (red) and nuclei (blue). Scale bar 20 µm. (For interpretation of the references to colour in this figure legend, the reader is referred to the web version of this article.)

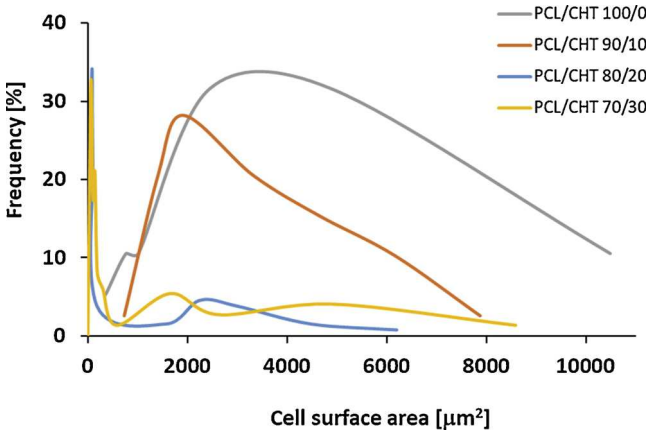

Fig. 5. Frequency distributions of cell surface area on the PCL/CHT double porous membranes.

enzyme to enter inside the hydrophobic and crystalline PCL chains. Decreasing the concentration of PCL wt% the degradation increases as CHT chains decrease the crystallinity of PCL chains and also increase the hydrophilicity of the overall blends, creating more space for the enzymatic solution to invade inside the PCL chains [27]. Moreover, increasing the macrovoids size and porosity, the enzyme can have a direct access inside the bulk leading to weight loss of 95% of PCL/CHT 70/30 within 10 days. On the other hand, the degradation kinetics by using lysozyme was quite straightforward despite the increase of macrovoids and porosity.

The bioactivity of 3D scaffolds used in tissue engineering applications depends on density of the available ligands, scaffolds microstructural environment at which specific cell binding occurs. Ligand density is defined by the composition of the scaffolds and the ligand density on the surface is inversely proportional to the surface macrovoid size or proportional to the effective surface area, surface which is exposed for initial attachment of the cells.

The physico-chemical and structural properties of the developed double porous membrane scaffolds, ultimately strongly affected the cellular morpho-functional behaviour and invasion in the polymeric scaffold bulk which is also supported by our previous study [28]. Our results are in line with other studies that show the viability of stem cells

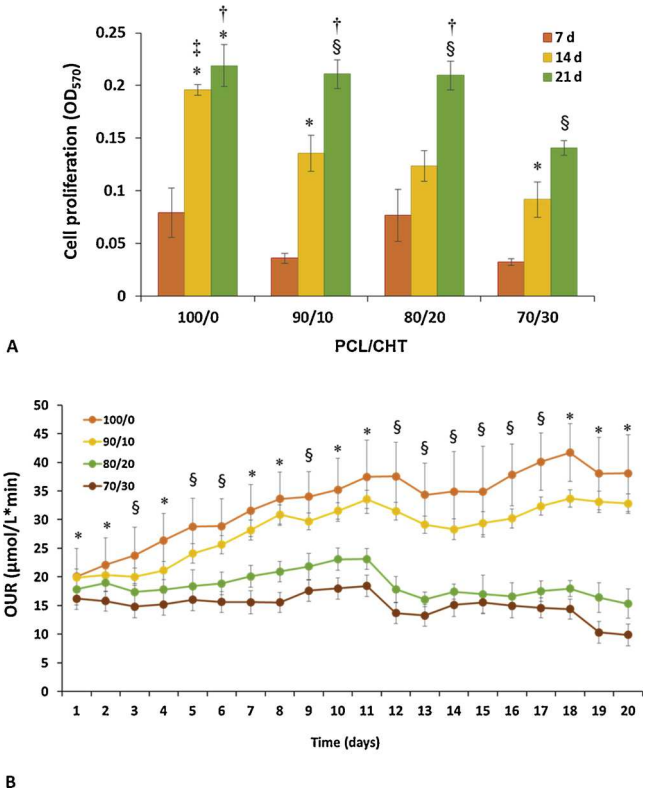

Fig. 7. Cell proliferation (A) and oxygen uptake rate (B) of hMSCs at different days of culture on PCL/CHT 100/0, 90/10, 80/20, 70/30 double porous membranes. Data statistically significant according to ANOVA followed by Bonferroni t'test ($p < 0.05$): A) (*) vs 7 days, (§) vs 7 and 14 days, on the same substrate; (†) vs 70/30, (‡) vs all, at the same day of culture. B) (*) 100/0 vs all, 90/10 vs 80/20 and 70/30, and 80/20 vs 70/30; (§) 100/0 vs all, 90/10 vs 80/20 and 70/30, at the same day of culture.

affected by geometry and morphological structure of the scaffolds, which modulate the cell shape and cytoskeletal tension thus regulating cell functions [29]. In our case, the membrane porosity and ESA were responsible of the different morphology displayed by cells on the

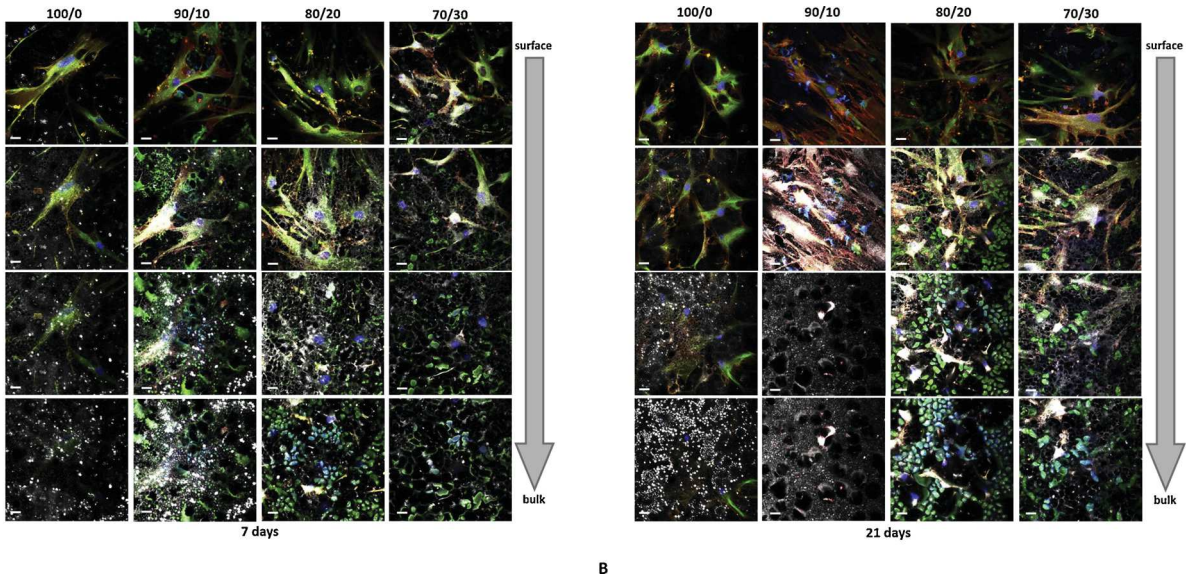

Fig. 6. Distribution in the z-axis of vimentin (green), CD90 (red), nuclei (blue) and scaffolds (grey) after 7 (a) and 21 (b) days of hMSC culture on PCL/CHT double porous membranes. CLSM images were collected from the surface to the bulk in the z-scan mode at step size intervals of 5 μm. Scale bar 20 μm. (For interpretation of the references to colour in this figure legend, the reader is referred to the web version of this article.)

scaffolds. The increase of surface macrovoids size with consequent decrease of ESA% in the blended PCL/CHT membranes (e.g., PCL/CHT 80/20, PCL/CHT 70/30) reduced the cell adhesion on the surface enhancing the invasion of cells into the bulk that assume a more globular shape. Additionally, the increase of CHT wt% in such membranes causes also an increase of micropore size distribution and surface porosity that are responsible of higher irregular surface. We found on PCL/CHT 80/20 and PCL/CHT 70/30 high percentage of cells entrapped inside the macrovoids that exhibit a spherical morphology. Differently, lower surface porosity conferred more regular and smoother surfaces, that in addition to higher ESA, enhanced the adhesion of hMSCs on the membrane surfaces as occurred on PCL/CHT 100/0 and PCL/CHT 90/10 scaffolds. Indeed, cells adhered on the surface of these membranes achieving a wide spreading. The cell invasion in the double porous membrane scaffolds reduced the cell proliferation that was lower on scaffolds with increase of CHT wt%, which lead to the formation of greater macrovoids and a more porous surface. These results are corroborated by previous findings reported by O'Brien et al. [9] that shown a strong correlation between the scaffold specific surface area and cell attachment, and by Murphy et al. [10] that highlighted the important role played by the scaffold specific surface area on initial cell adhesion.

In our study, the proliferation rate increased in the time consistently to the scaffold degradation, reaching maximum values after 21 days on all membrane scaffolds especially for hMSCs cultured on PCL/CHT 100/0, 90/10 and 80/20. A further evidence is provided by the OUR data that show a similar trend of cell proliferation. In particular, cellular oxygen consumption is a good indicator of cell viability and functions since the oxygen is one of the most important nutrients for cells and play an important role in regulating MSCs function [30,31]. The OUR of the hMSCs cultured on the blends increased in the time and with the PCL wt% coherently with cell adhesion and proliferation data highlighting an enhanced cellular metabolic activity.

Overall the results demonstrated that the scaffolds were able to create a permissive environment for hMSC adhesion and invasion affecting their morphology, proliferation and metabolism and maintaining their viability and integrity. The macrovoids enabled the cell invasion into the membrane and the microporosity ensured an adequate diffusive mass transfer of nutrients and metabolites, which are essential for the long-term maintenance of cell viability and functions.

5. Conclusions

In this study, we developed new double porous membrane scaffolds consisting of variable macrovoids interconnected through microporous structure. We found a linear change in scaffolds macrovoids size, effective surface area and surface irregularity by changing the PCL/CHT blend, which has a direct impact on their physico-chemical and degradation properties.

Topographical structure of the membrane scaffolds significantly influenced the morpho-functional behavior of hMSCs. Cell viability and proliferation increased by decreasing macrovoid size and by increasing the effective surface area, which is available for specific integrin-ligand interaction. Cells adhered and proliferated on the surface of PCL/CHT 100/0 and PCL/CHT 90/10 membranes, that are characterized by a high effective surface area and small macrovoids. PCL/CHT 80/20 and PCL/CHT 70/30 enabled the entrapment of cells inside the large macrovoids owing to a limited effective surface area. These results provided evidence that the three-dimensional double porous membrane scaffolds offer physical, chemical and mechanical cues for hMSCs attachment and proliferation. Specifically, PCL/CHT 80/20 membrane is characterised by topographical, mechanical and degradation properties that promote long-term cell viability in a culture environment where cells can invade and proliferate inside the macrovoids, which are characterized by a microporous structure that modulate mass transfer of molecules. These properties make the membrane suitable to open new possibility for stem cell based tissue engineering (e.g., liver, vessels). Ultimately, this membrane scaffold can provide a selective cell co-culture model for different tissues where, according to the cellular dimension, cells can invade and proliferate inside the macrovoids and/or can adhere on the surface ensuring the biochemical cross-talk, which is necessary for recapitulating physiological functions.

Declaration of Competing Interest

The authors declare no conflict of interests.

Acknowledgements

The author would like to acknowledge the funding organisation Erasmus mundus doctorate in membrane engineering-5th Ed. under European commission (EACEA).

Appendix A. Supplementary data

Supplementary material related to this article can be found, in the online version, at doi:https://doi.org/10.1016/j.colsurfb.2019.110493.

References

[1] S. Salerno, E. Curcio, A. Bader, L. Giorno, E. Drioli, L. De Bartolo, Gas permeable membrane bioreactor for the co-culture of human skin derived mesenchymal stem cells with hepatocytes and endothelial cells, J. Memb. Sci. 563 (2018) 694–707, https://doi.org/10.1016/j.memsci.2018.06.029.
[2] A. Piscioneri, S. Morelli, M. Mele, M. Canonaco, E. Bilotta, P. Pantano, E. Drioli, L. De Bartolo, Neuroprotective effect of human mesenchymal stem cells in a compartmentalized neuronal membrane system, Acta Biomater. 24 (2015) 297–308, https://doi.org/10.1016/j.actbio.2015.06.013.
[3] A. Di Luca, B. Ostrowska, I. Lorenzo-Moldero, A. Lepedda, W. Swieszkowski, C. Van Blitterswijk, L. Moroni, Gradients in pore size enhance the osteogenic differentiation of human mesenchymal stromal cells in three-dimensional scaffolds, Sci. Rep. 6 (2016) 22898, https://doi.org/10.1038/srep22898.
[4] P. Kasten, I. Beyen, P. Niemeyer, R. Luginbühl, M. Bohner, W. Richter, Porosity and pore size of β-tricalcium phosphate scaffold can influence protein production and osteogenic differentiation of human mesenchymal stem cells: an in vitro and in vivo study, Acta Biomater. 4 (2008) 1904–1915, https://doi.org/10.1016/j.actbio.2008.05.017.
[5] S. Morelli, S. Salerno, H.M.M. Ahmed, A. Piscioneri, L. De Bartolo, Recent strategies combining biomaterials and stem cells for bone, liver and skin regeneration, Curr. Stem Cell Res. Ther. 11 (2016) 676–691, https://doi.org/10.2174/1574888X11666160201120004.
[6] S. Salerno, S. Morelli, L. De Bartolo, Advanced membrane systems for tissue engineering, Curr. Org. Chem. 21 (2017) 1760–1774, https://doi.org/10.2174/1385272820666160617092944.
[7] H.M.M. Ahmed, S. Salerno, S. Morelli, L. Giorno, L. De Bartolo, 3D liver membrane system by co-culturing human hepatocytes, sinusoidal endothelial and stellate cells, Biofabrication. 9 (2017) 025022, https://doi.org/10.1088/1758-5090/aa70c7.
[8] E. Drioli, L. De Bartolo, Membrane bioreactor for cell tissues and organoids, Artif. Organs 30 (2006) 793–802, https://doi.org/10.1111/j.1525-1594.2006.00302.x.
[9] F.J. O'Brien, B.A. Harley, I.V. Yannas, L.J. Gibson, The effect of pore size on cell adhesion in collagen-GAG scaffolds, Biomaterials 26 (2005) 433–441, https://doi.org/10.1016/j.biomaterials.2004.02.052.
[10] C.M. Murphy, M.G. Haugh, F.J. O'Brien, The effect of mean pore size on cell attachment, proliferation and migration in collagen–glycosaminoglycan scaffolds for bone tissue engineering, Biomaterials 31 (2010) 461–466, https://doi.org/10.1016/j.biomaterials.2009.09.063.
[11] M. Dufresne, P. Bacchin, G. Cerino, J.C. Remigy, G.N. Adrianus, P. Aimar, C. Legallais, Human hepatic cell behavior on polysulfone membrane with double porosity level, J. Memb. Sci. 428 (2013) 454–461, https://doi.org/10.1016/j.memsci.2012.10.041.
[12] S. Salerno, A. Messina, F. Giordano, A. Bader, E. Drioli, L. De Bartolo, Dermal-epidermal membrane systems by using human keratinocytes and mesenchymal stem cells isolated from dermis, Mater. Sci. Eng. C 71 (2017) 943–953, https://doi.org/10.1016/j.msec.2016.11.008.
[13] S. Salerno, S. Morelli, F. Giordano, A. Gordano, L. De Bartolo, Polymeric membranes modulate human keratinocyte differentiation in specific epidermal layers, Colloids Surf. B: Biointerfaces 146 (2016) 352–362, https://doi.org/10.1016/j.colsurfb.2016.06.026.
[14] S.C. Neves, L.S. Moreira Teixeira, L. Moroni, R.L. Reis, C.A. Van Blitterswijk, N.M. Alves, M. Karperien, J.F. Mano, Chitosan/poly(ε-caprolactone) blend scaffolds for cartilage repair, Biomaterials 32 (2011) 1068–1079, https://doi.org/10.1016/j.biomaterials.2010.09.073.
[15] S. Mitragotri, J. Lahann, Physical approaches to biomaterial design, Nat. Mater. 8 (2009) 15, https://doi.org/10.1038/nmat2344.
[16] M.A. Meyers, J. McKittrick, P.-Y. Chen, Structural biological materials: critical mechanics-materials connections, Science 339 (2013) 773–779, https://doi.org/10.

1126/science.1220854.
[17] S. Morelli, S. Salerno, M. Rende, L.C. Lopez, P. Favia, A. Procino, B. Memoli, V.E. Andreucci, R. d'Agostino, E. Drioli, L. De Bartolo, Human hepatocyte functions in a galactosylated membrane bioreactor, J. Memb. Sci. 302 (2007), https://doi.org/10.1016/j.memsci.2007.06.027.
[18] L. De Bartolo, A. Piscioneri, G. Cotroneo, S. Salerno, F. Tasselli, C. Campana, S. Morelli, M. Rende, M.C. Caroleo, M. Bossio, E. Drioli, Human lymphocyte PEEK-WC hollow fiber membrane bioreactor, J. Biotechnol. 132 (2007), https://doi.org/10.1016/j.jbiotec.2007.08.040.
[19] J. Aragón, S. Salerno, L. De Bartolo, S. Irusta, G. Mendoza, Polymeric electrospun scaffolds for bone morphogenetic protein 2 delivery in bone tissue engineering, J. Colloid Interface Sci. 531 (2018) 126–137, https://doi.org/10.1016/j.jcis.2018.07.029.
[20] J.C. Remigy, M. Meireles, X. Thibault, Morphological characterization of a polymeric microfiltration membrane by synchrotron radiation computed microtomography, J. Memb. Sci. 305 (2007) 27–35, https://doi.org/10.1016/j.memsci.2007.06.059.
[21] A.D. Olubamiji, Z. Izadifar, J.L. Si, D.M.L. Cooper, B.F. Eames, D.X. Chen, Modulating mechanical behaviour of 3D-printed cartilage-mimetic PCL scaffolds: influence of molecular weight and pore geometry, Biofabrication 8 (2016) 25020, https://doi.org/10.1088/1758-5090/8/2/025020.
[22] V.M. Correlo, L.F. Boesel, M. Bhattacharya, J.F. Mano, N.M. Neves, R.L. Reis, Properties of melt processed chitosan and aliphatic polyester blends, Mater. Sci. Eng. A 403 (2005) 57–68, https://doi.org/10.1016/j.msea.2005.04.055.
[23] H.S. Azevedo, R.L. Reis, Understanding the enzymatic degradation of biodegradable polymers and strategies to control their degradation rate, in: R.L. Reis, J. San Román (Eds.), Biodegradable Systems in Tissue Engineering and Regenerative Medicine, CRC Press, 2005, pp. 177–201, , https://doi.org/10.1201/9780203491232.ch12.
[24] A. Anitha, S. Sowmya, P.T.S. Kumar, S. Deepthi, K.P. Chennazhi, H. Ehrlich, M. Tsurkan, R. Jayakumar, Chitin and chitosan in selected biomedical applications, Prog. Polym. Sci. 39 (2014) 1644–1667, https://doi.org/10.1016/j.progpolymsci.2014.02.008.
[25] T. Honma, L. Zhao, N. Asakawa, Y. Inoue, Poly(ε-caprolactone)/chitin and poly(ε-caprolactone)/chitosan blend films with compositional gradients: fabrication and their biodegradability, Macromol. Biosci. 6 (2006) 241–249, https://doi.org/10.1002/mabi.200500216.
[26] R.J. Mondschein, A. Kanitkar, C.B. Williams, S.S. Verbridge, T.E. Long, Polymer structure-property requirements for stereolithographic 3D printing of soft tissue engineering scaffolds, Biomaterials 140 (2017) 170–188, https://doi.org/10.1016/j.biomaterials.2017.06.005.
[27] F. He, S. Li, M. Vert, R. Zhuo, Enzyme-catalyzed polymerization and degradation of copolymers prepared from ε-caprolactone and poly(ethylene glycol), Polymer 44 (2003) 5145–5151, https://doi.org/10.1016/S0032-3861(03)00562-7.
[28] P. Bacchin, P. Das, A. van der Meer, A. Vivas, Y.B. Arik, J.-C. Remigy, J.-F. Lahitte, R.G.H. Lammertink, Tunable microstructured membranes in organs-on-chips to monitor transendothelial hydraulic resistance, Tissue Eng. Part A (2019), https://doi.org/10.1089/ten.TEA.2019.0021 In press.
[29] X. Kang, Y. Xie, H.M. Powell, L. James Lee, M.A. Belury, J.J. Lannutti, D.A. Kniss, Adipogenesis of murine embryonic stem cells in a three-dimensional culture system using electrospun polymer scaffolds, Biomaterials 28 (2007) 450–458, https://doi.org/10.1016/j.biomaterials.2006.08.052.
[30] G. Muschler, C. Nakamoto, L. Griffith, Engineering Principles of Clinical Cell-Based Tissue Engineering, (2004), https://doi.org/10.2106/00004623-200407000-00029.
[31] A. Nuschke, M. Rodrigues, A.W. Wells, K. Sylakowski, A. Wells, Mesenchymal stem cells/multipotent stromal cells (MSCs) are glycolytic and thus glucose is a limiting factor of in vitro models of MSC starvation, Stem Cell Res. Ther. 7 (2016) 179, https://doi.org/10.1186/s13287-016-0436-7.